

REVISITING NOISE SCHEDULE DESIGN FOR DIFFUSION TRAINING

Tiankai Hang*
Southeast University
tkhang@seu.edu.cn

Shuyang Gu
Microsoft Research Asia
cientgu@gmail.com

Xin Geng†
Southeast University
xgeng@seu.edu.cn

Baining Guo†
Southeast University & Microsoft Research Asia
307000167@seu.edu.cn

ABSTRACT

Diffusion models have emerged as the de facto choice for generating high-quality visual signals across various domains. However, training a single model to predict noise across various levels poses significant challenges, necessitating numerous iterations and incurring significant computational costs. Various approaches, such as loss weighting strategy design and architectural refinements, have been introduced to expedite convergence and improve model performance. In this study, we propose a novel approach to design the noise schedule for enhancing the training of diffusion models. Our key insight is that importance sampling of log SNR, equivalent to a modified noise schedule, improves training efficiency by focusing around $\log \text{SNR} = 0$. This sampling helps the model focus on the critical transition between signal and noise dominance, leading to more robust predictions. We empirically demonstrate the superiority of our noise schedule over the standard cosine schedule. Furthermore, our noise schedule shows consistent improvements on ImageNet across different prediction targets.

1 INTRODUCTION

Diffusion models have emerged as a pivotal technique for generating high-quality visual signals across diverse domains, including image synthesis (Ramesh et al., 2022; Saharia et al., 2022; Rombach et al., 2022), video generation (Ho et al., 2022; Singer et al., 2023; Brooks et al., 2024), and even 3D object generation (Wang et al., 2022; Nichol et al., 2022). One of the key strengths of diffusion models lies in their ability to approximate complex distributions, where Generative Adversarial Networks (GANs) may encounter difficulties. Despite the substantial computational resources and numerous training iterations required for convergence, improving the training efficiency of diffusion models is essential for their application in large-scale scenarios, such as high-resolution image synthesis and long video generation.

Recent efforts to enhance diffusion model training efficiency have primarily focused on two directions. The first approach centers on architectural improvements. For instance, the use of Adaptive Layer Normalization (Gu et al., 2022), when combined with zero initialization in the Transformer architecture Peebles & Xie (2023), has shown promising results. MM-DiT (Esser et al., 2024) extends this approach to multi-modality by employing separate weights for vision and text processing. Similarly, U-shaped skip connections within Transformers (Hoogeboom et al., 2023; Bao et al., 2022; Crowson et al., 2024) and reengineered layer designs (Karras et al., 2024) have contributed to more efficient learning processes.

The second direction explores various loss weighting strategies to accelerate training convergence. Works such as eDiff-I (Balaji et al., 2022) and Ernie-ViLG 2.0 (Feng et al., 2022) address training difficulties across noise intensities using a Mixture of Experts approach. Other studies have investigated prioritizing specific noise levels (Choi et al., 2022) and reducing weights of noisy tasks (Hang

*Long-term researcher intern at Microsoft Research Asia. †Corresponding authors.

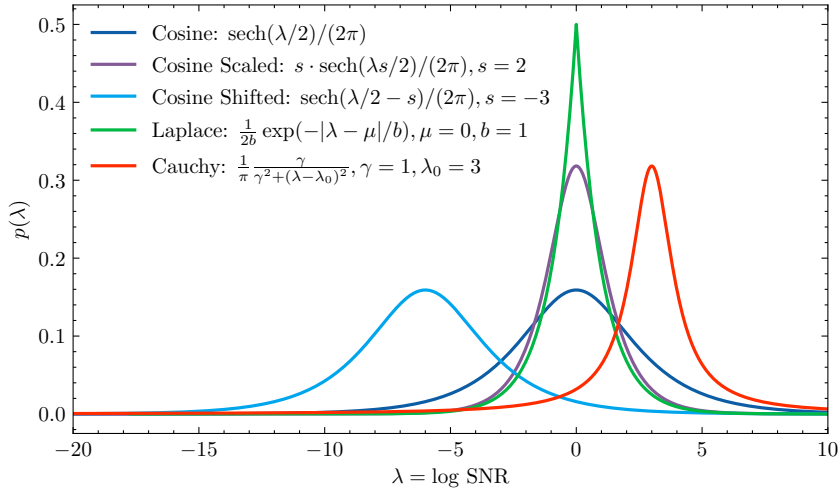


Figure 1: Illustration of the probability density functions of different noise schedules.

et al., 2023) to enhance learning effectiveness. Recent developments include a softer weighting approach for high-resolution image synthesis (Crowson et al., 2024) and empirical findings on the importance of intermediate noise intensities (Esser et al., 2024).

Despite these advances, the fundamental role of noise scheduling in diffusion model training remains underexplored. In this study, we present a novel approach focusing on the fundamental role of noise scheduling, which is a function that determines how much noise is added to the input data at each timestep t during the training process, controlling the distribution of noise levels that the neural network learns to remove. Our framework provides a unified perspective for analyzing noise schedules and importance sampling, leading to a straightforward method for designing noise schedules through the identification of curves in the $p(\lambda)$ distribution, as visualized in Figure 1. Empirical analysis shows that allocating more computation to mid-range noise levels (around $\log \text{SNR} = 0$) performs better than increasing loss weights, especially with limited computational budgets.

We evaluate noise schedules, including Laplace, Cauchy, and Cosine Shifted/Scaled variants, on ImageNet with 500K iterations (about 100 epochs). Our results, measured using the Fréchet Inception Distance (FID) metric at both 256×256 and 512×512 resolutions, demonstrate that noise schedules with concentrated probability density around $\log \text{SNR} = 0$ consistently outperform alternatives, with the Laplace schedule showing particularly favorable performance.

The key contributions of our work can be summarized as follows:

- A unified framework for analyzing and designing noise schedules in diffusion models, offering a more systematic approach to noise schedule optimization.
- Empirical evidence demonstrating the superiority of mid-range noise level focus over loss weight adjustments for improving training efficiency.
- Comprehensive evaluation and comparison of various noise schedules, providing practical guidelines for future research and applications in diffusion model training.

2 METHOD

2.1 PRELIMINARIES

Diffusion models (Ho et al., 2020; Yang et al., 2021) learn to generate data by iteratively reversing the diffusion process. We denote the distribution of data points as $\mathbf{x} \sim p_{\text{data}}(\mathbf{x})$. The diffusion process systematically introduces noise to the data in a progressive manner. In a continuous setting, the noisy data at timestep t is defined as follows:

$$\mathbf{x}_t = \alpha_t \mathbf{x} + \sigma_t \epsilon, \quad \text{where } \epsilon \sim \mathcal{N}(0, \mathbf{I}), \quad (1)$$

where α_t and σ_t are the coefficients of the adding noise process, essentially representing the noise schedule. For the commonly used prediction target velocity: $\mathbf{v}_t = \alpha_t \epsilon - \sigma_t \mathbf{x}$ (Salimans & Ho,

2022), the diffusion model \mathbf{v}_θ is trained through the Mean Squared Error (MSE) loss:

$$\mathcal{L}(\theta) = \mathbb{E}_{\mathbf{x} \sim p_{\text{data}}(\mathbf{x})} \mathbb{E}_{t \sim p(t)} \left[w(t) \|\mathbf{v}_\theta(\alpha_t \mathbf{x} + \sigma_t \boldsymbol{\epsilon}, t, \mathbf{c}) - \mathbf{v}_t\|_2^2 \right], \quad (2)$$

where $w(t)$ is the loss weight, \mathbf{c} denotes the condition information. In the context of class-conditional generation tasks, \mathbf{c} represents the class label. Common practices sample t from the uniform distribution $\mathcal{U}[0, 1]$. Kingma et al. (2021) introduced the Signal-to-Noise ratio as $\text{SNR}(t) = \frac{\alpha_t^2}{\sigma_t^2}$ to measure the noise level of different states. Notably, $\text{SNR}(t)$ monotonically decreases with increasing t . Some works represent the loss weight from the perspective of SNR (Salimans & Ho, 2022; Hang et al., 2023; Crowson et al., 2024). To simplify, we denote $\lambda = \log \text{SNR}$ to indicate the noise intensities. In the Variance Preserving (VP) setting, the coefficients in Equation 1 can be calculated by $\alpha_t^2 = \frac{\exp(\lambda)}{\exp(\lambda)+1}$, $\sigma_t^2 = \frac{1}{\exp(\lambda)+1}$.

While these foundational concepts have advanced diffusion models, the choice of noise schedule remains somewhat ad hoc. This motivates us to develop a more systematic framework for analyzing and designing noise schedules by examining them from a probability perspective.

2.2 NOISE SCHEDULE DESIGN FROM A PROBABILITY PERSPECTIVE

The training process of diffusion models involves sampling timesteps t from a uniform distribution. However, this uniform sampling in time actually implies a non-uniform sampling of noise intensities. We can formalize this relationship through the lens of importance sampling (Bishop & Nasrabadi, 2006). Specifically, when t follows a uniform distribution, the sampling probability of noise intensity λ is given by:

$$p(\lambda) = p(t) \left| \frac{dt}{d\lambda} \right| = -\frac{dt}{d\lambda}, \quad (3)$$

where the negative sign appears because λ monotonically decreases with t . We take cosine noise schedule (Nichol & Dhariwal, 2021) as an example, where $\alpha_t = \cos(\frac{\pi t}{2})$, $\sigma_t = \sin(\frac{\pi t}{2})$. Then we can deduce that $\lambda = -2 \log \tan(\pi t/2)$ and $t = 2/\pi \arctan e^{-\lambda/2}$. Thus the distribution of λ is: $p(\lambda) = -dt/d\lambda = \text{sech}(\lambda/2)/2\pi$. This derivation illustrates the process of obtaining $p(\lambda)$ from a noise schedule $\lambda(t)$. On the other hand, we can derive the noise schedule from the sampling probability of different noise intensities $p(\lambda)$. By integrating Equation 3, we have:

$$t = 1 - \int_{-\infty}^{\lambda} p(\lambda) d\lambda = \mathcal{P}(\lambda), \quad (4)$$

$$\lambda = \mathcal{P}^{-1}(t), \quad (5)$$

where $\mathcal{P}(\lambda)$ represents the cumulative distribution function of λ . Thus we can obtain the noise schedule λ by applying the inverse function \mathcal{P}^{-1} . In conclusion, during the training process, the importance sampling of varying noise intensities essentially equates to the modification of the noise schedules. To illustrate this concept, let's consider the Laplace distribution as an example, we can derive the cumulative distribution function $\mathcal{P}(\lambda) = 1 - \int_{\frac{1}{2b}}^{\lambda} \exp(-|\lambda - \mu|/b) d\lambda = \frac{1}{2} (1 + \text{sgn}(\lambda - \mu)(1 - \exp(-|\lambda - \mu|/b)))$. Subsequently, we can obtain the inverse function to express the noise schedule in terms of λ : $\lambda = \mu - b \text{sgn}(0.5 - t) \ln(1 - 2|t - 0.5|)$. Here, $\text{sgn}(\cdot)$ denotes the signum function, which equals 1 for positive inputs, -1 for negative inputs. The pseudo-code for implementing the Laplace schedule in the training of diffusion models is presented in A.1.

This framework reveals that noise schedule design can be reframed as a probability distribution design problem. Rather than directly specifying how noise varies with time, we can instead focus on how to optimally distribute our sampling across different noise intensities. Our approach is also applicable to the recently popular flow matching with logit normal sampling scheme (Esser et al., 2024). Within our framework, we analyzed the distribution of its logSNR in A.5 and demonstrated its superiority over vanilla flow matching and cosine scheduling from the perspective of $p(\lambda)$.

2.3 UNIFIED FORMULATION FOR DIFFUSION TRAINING

VDM++ (Kingma & Gao, 2023) proposes a unified formulation that encompasses recent prominent frameworks and loss weighting strategies for training diffusion models, as detailed below:

$$\mathcal{L}_w(\theta) = \frac{1}{2} \mathbb{E}_{\mathbf{x} \sim \mathcal{D}, \boldsymbol{\epsilon} \sim \mathcal{N}(0, \mathbf{I}), \lambda \sim p(\lambda)} \left[\frac{w(\lambda)}{p(\lambda)} \|\hat{\boldsymbol{\epsilon}}_\theta(\mathbf{x}_\lambda; \lambda) - \boldsymbol{\epsilon}\|_2^2 \right], \quad (6)$$

Noise Schedule	$p(\lambda)$	$\lambda(t)$
Cosine	$\text{sech}(\lambda/2)/2\pi$	$2 \log(\cot(\frac{\pi t}{2}))$
Laplace	$e^{-\frac{ \lambda-\mu }{b}}/2b$	$\mu - b \text{sgn}(0.5 - t) \log(1 - 2 t - 0.5)$
Cauchy	$\frac{1}{\pi} \frac{\gamma}{(\lambda-\mu)^2 + \gamma^2}$	$\mu + \gamma \tan(\frac{\pi}{2}(1 - 2t))$
Cosine Shifted	$\frac{1}{2\pi} \text{sech}(\frac{\lambda-\mu}{2})$	$\mu + 2 \log(\cot(\frac{\pi t}{2}))$
Cosine Scaled	$\frac{s}{2\pi} \text{sech}(\frac{s\lambda}{2})$	$\frac{2}{s} \log(\cot(\frac{\pi t}{2}))$

Table 1: Overview of various Noise Schedules. The table categorizes them into five distinct types: Cosine, Laplace, Cauchy, and two variations of Cosine schedules. The second column $p(\lambda)$ denotes the sampling probability at different noise intensities λ . The last column $\lambda(t)$ indicates how to sample noise intensities for training. We derived their relationship in Equation 3 and 5.

where \mathcal{D} signifies the training dataset, noise ϵ is Gaussian noise, and $p(\lambda)$ is the distribution of noise intensities. This formulation offers a flexible framework for various diffusion training strategies. Predicting targets like \mathbf{x}_0 and \mathbf{v} can be re-parameterized to ϵ -prediction. $w(\lambda)$ denotes the loss weighting strategy. Although adjusting $w(\lambda)$ is theoretically equivalent to altering $p(\lambda)$. In practice, directly modifying $p(\lambda)$ to concentrate computational resources on training specific noise levels is more effective than enlarging the loss weight on specific noise levels. Our research focuses on how to design an optimal $p(\lambda)$ that can effectively allocate computational resources across different noise levels. By carefully crafting the distribution of noise intensities, we aim to improve the overall training process and the quality of the resulting diffusion models. With the unified formulation providing a flexible framework for diffusion training, we can now apply these theoretical insights to practical settings. By carefully designing the distribution of noise intensities, we can optimize the training process and improve the performance of diffusion models in real-world applications. In the following section, we explore practical noise schedule strategies to achieve better results.

2.4 PRACTICAL SETTINGS

Stable Diffusion 3 (Esser et al., 2024), EDM (Karras et al., 2022), and Min-SNR (Hang et al., 2023; Crowson et al., 2024) find that the denoising tasks with medium noise intensity is most critical to the overall performance of diffusion models. Therefore, we increase the probability of $p(\lambda)$ when λ is of moderate size, and obtain a new noise schedule according to Section 2.2.

Specifically, we investigate four novel noise strategies, named Cosine Shifted, Cosine Scaled, Cauchy, and Laplace respectively. The detailed setting are listed in Table 1. Cosine Shifted use μ to explore where the maximum probability should be used. Cosine Scaled explores how much the noise probability should be increased under the use of Cosine strategy to achieve better results. The Cauchy distribution adjusts both amplitude and offset. The Laplace distribution is characterized by its mean μ and scale b , controls both the magnitude of the probability and the degree of concentration of the distribution. These strategies contain several hyperparameters, which we will explore in Section 3.5. Unless otherwise stated, we report the best hyperparameter results.

By re-allocating the computation resources at different noise intensities, we can train the complete denoising process. During sampling process, we align the sampled SNRs as the cosine schedule to ensure a fair comparison. Specifically, first we sample $\{t_0, t_1, \dots, t_s\}$ from uniform distribution $\mathcal{U}[0, 1]$, then get the corresponding SNRs from Cosine schedule: $\{\frac{\alpha_{t_0}^2}{\sigma_{t_0}^2}, \frac{\alpha_{t_1}^2}{\sigma_{t_1}^2}, \dots, \frac{\alpha_{t_s}^2}{\sigma_{t_s}^2}\}$. According to Equation 5, we get the corresponding $\{t'_0, t'_1, \dots, t'_s\}$ by inverting these SNR values through the respective noise schedules. Finally, we use DDIM (Song et al., 2021) to sample with these new calculated $\{t'\}$. It is important to note that, from the perspective of the noise schedule, how to allocate the computation resource during inference is also worth reconsideration. We will not explore it in this paper and leave this as future work.

3 EXPERIMENTS

3.1 IMPLEMENTATION DETAILS

Dataset. We conduct experiments on ImageNet (Deng et al., 2009) with 256×256 and 512×512 resolution. For each image, we follow the preprocessing in Rombach et al. (2022) to center crop

Method	$w(\lambda)$	$p(\lambda)$
Cosine	$e^{-\lambda/2}$	$\text{sech}(\lambda/2)$
Min-SNR	$e^{-\lambda/2} \cdot \min\{1, \gamma e^{-\lambda}\}$	$\text{sech}(\lambda/2)$
Soft-Min-SNR	$e^{-\lambda/2} \cdot \gamma / (e^\lambda + \gamma)$	$\text{sech}(\lambda/2)$
FM-OT	$(1 + e^{-\lambda})\text{sech}^2(\lambda/4)$	$\text{sech}^2(\lambda/4)/8$
EDM	$(1 + e^{-\lambda})(0.5^2 + e^{-\lambda})\mathcal{N}(\lambda; 2.4, 2.4^2)$	$(0.5^2 + e^{-\lambda})\mathcal{N}(\lambda; 2.4, 2.4^2)$

Table 2: Comparison of different methods and related loss weighting strategies (as in Equation 6).

and encode images to latents. The resulting compressed latents have dimensions of $32 \times 32 \times 4$ for 256^2 images and $64 \times 64 \times 4$ for 512^2 images, effectively reducing the spatial dimensions while preserving essential visual information.

Network Architecture. We adopt DiT-B from Peebles & Xie (2023) as our backbone. We replace the last AdaLN Linear layer with vanilla linear. Others are kept the same as the original implementation. The patch size is set to 2 and the projected sequence length of $32 \times 32 \times 4$ is $\frac{32}{2} \cdot \frac{32}{2} = 256$. The class condition is injected through the adaptive layernorm. In this study, our primary objective is to demonstrate the effectiveness of our proposed noise schedule compared to existing schedules under a fixed training budget, rather than to achieve state-of-the-art results. Consequently, we do not apply our method to extra-large (XL) scale models.

Training Settings. We adopt the Adam optimizer (Kingma & Ba, 2014) with constant learning rate 1×10^{-4} . We set the batch size to 256 following Peebles & Xie (2023) and Gao et al. (2023). Each model is trained for 500K iterations (about 100 epochs) if not specified. Our implementation is primarily based on OpenDiT (Zhao et al., 2024) and experiments are mainly conducted on $8 \times 16G$ V100 GPUs. Different from the default discrete diffusion setting with linear noise schedule in the code base, we implement the diffusion process in a continuous way. Specifically, we sample t from uniform distribution $\mathcal{U}[0, 1]$.

Baselines and Metrics. We compare our proposed noise schedule with several baseline settings in Table 2. For each setting, we sample images using DDIM (Song et al., 2021) with 50 steps. Despite the noise strategy for different settings may be different, we ensure they share the same $\lambda = \log \text{SNR}$ at each sampling step. This approach is adopted to exclusively investigate the impact of the noise strategy during the training phase. Moreover, we report results with different classifier-free guidance scales (Ho & Salimans, 2021), and the FID is calculated using 10K generated images. We select the optimal one to better evaluate the actual performance of different models.

3.2 COMPARISON WITH BASELINE SCHEDULES AND LOSS WEIGHT DESIGNS

This section details the principal findings from our experiments on the ImageNet-256 dataset, focusing on the comparative effectiveness of various noise schedules and loss weightings in the context of CFG values. Table 3 illustrates these comparisons, showcasing the performance of each method in terms of the FID-10K score.

The experiments reveal that our proposed noise schedules, particularly *Laplace*, achieve the most notable improvements over the traditional cosine schedule, as indicated by the bolded best scores and the blue numbers representing the reductions compared to baseline’s best score of 10.85.

We also provide a comparison with methods that adjust the loss weight, including *Min-SNR* and *Soft-Min-SNR*. Unless otherwise specified, the hyperparameter γ for both loss weighting schemes is set to 5. We find that although these methods can achieve better results than the baseline, they are still not as effective as our method of modifying the noise schedule. This indicates that deciding where to allocate more computational resources is more efficient than adjusting the loss weight. Compared with other noise schedules like EDM (Karras et al., 2022) and Flow Matching (Lipman et al., 2022), we found that no matter which CFG value, our results significantly surpass theirs under the same training iterations.

Furthermore, we investigate the convergence speed of these method, and the results are shown in Figure 2. It can be seen that adjusting the noise schedule converges faster than adjusting the loss

Method	CFG=1.5	CFG=2.0	CFG=3.0
Cosine (Nichol & Dhariwal, 2021)	17.79	10.85	11.06
EDM (Karras et al., 2022)	26.11	15.09	11.56
FM-OT (Lipman et al., 2022)	24.49	14.66	11.98
Min-SNR (Hang et al., 2023)	16.06	9.70	10.43
Soft-Min-SNR (Crowson et al., 2024)	14.89	9.07	10.66
Cosine Shifted (Hoogeboom et al., 2023)	19.34	11.67	11.13
Cosine Scaled	12.74	8.04	11.02
Cauchy	12.91	8.14	11.02
Laplace	16.69	9.04	7.96 (-2.89)

Table 3: Comparison of various noise schedules and loss weightings on ImageNet-256, showing the performance (in terms of FID-10K) of different methods under different CFG values. The best results highlighted in bold and the blue numbers represent the improvement when compared with the baseline FID 10.85. The line in gray is our suggested noise schedule.

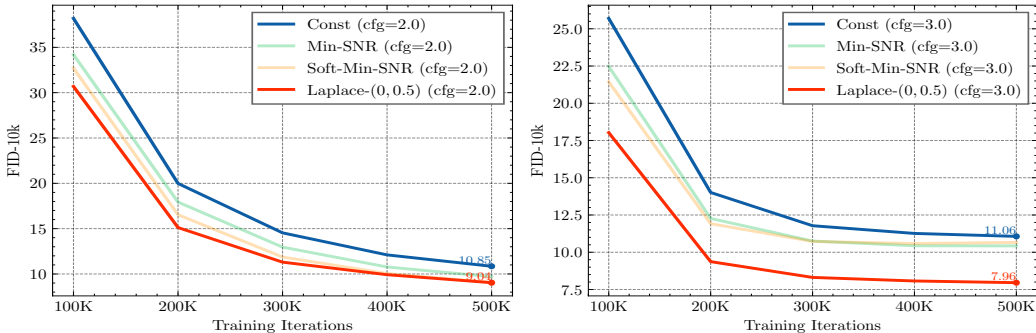


Figure 2: Comparison between adjusting the noise schedule, adjusting the loss weights and baseline setting. The Laplace noise schedule yields the best results and the fastest convergence speed.

weight. Additionally, we also notice that the optimal training method may vary when using different CFG values for inference, but adjusting the noise schedule generally yields better results.

3.3 ROBUSTNESS ON DIFFERENT PREDICTING TARGETS

We evaluate the effectiveness of our designed noise schedule across three commonly adopted prediction targets: ϵ , x_0 , and v . The results are shown in Table 4.

We observed that regardless of the prediction target, our proposed Laplace strategy significantly outperforms the Cosine strategy. It’s noteworthy that as the Laplace strategy focuses the computation on medium noise levels during training, the extensive noise levels are less trained, which could potentially affect the overall performance. Therefore, we have slightly modified the inference strategy of DDIM to start sampling from $t_{\max} = 0.99$.

Target	Noise Schedule	100K	200k	300k	400k	500k
x_0	Cosine	35.20	17.60	13.37	11.84	11.16
	Laplace (Ours)	21.78	10.86	9.44	8.73	8.48
v	Cosine	25.70	14.01	11.78	11.26	11.06
	Laplace (Ours)	18.03	9.37	8.31	8.07	7.96
ϵ	Cosine	28.63	15.80	12.49	11.14	10.46
	Laplace (Ours)	27.98	13.92	11.01	10.00	9.53

Table 4: Effectiveness on predicting targets: x_0 , ϵ , and v . The proposed *Laplace* schedule performs better than the baseline Cosine schedule along with training iterations.

	Cauchy(0, 0.5)	Cauchy(0, 1)	Cauchy(-1, 1)	Cauchy(1, 1)
CFG=1.5	12.91	14.32	18.12	16.60
CFG=2.0	8.14	8.93	10.38	10.19
CFG=3.0	11.02	11.26	10.81	10.94

Table 6: FID-10k results on ImageNet-256 with different Cauchy distribution parameters.

3.4 ROBUSTNESS ON HIGH RESOLUTION IMAGES

To explore the robustness of the adjusted noise schedule to different resolutions, we also designed experiments on Imagenet-512. As pointed out by Chen (2023), the adding noise strategy will cause more severe signal leakage as the resolution increases. Therefore, we need to adjust the hyperparameters of the noise schedule according to the resolution.

Specifically, the baseline Cosine schedule achieves the best performance when the CFG value equals to 3. So we choose this CFG value for inference. Through systematic experimentation, we explored the appropriate values for the Laplace schedule’s parameter b , testing within the range $\{0.5, 0.75, 1.0\}$, and determined that $b = 0.75$ was the most effective, resulting in an FID score of 9.09. This indicates that despite the need for hyperparameter tuning, adjusting the noise schedule can still stably bring performance improvements.

3.5 ABLATION STUDY

We conduct an ablation study to analyze the impact of hyperparameters on various distributions of $p(\lambda)$, which are enumerated below.

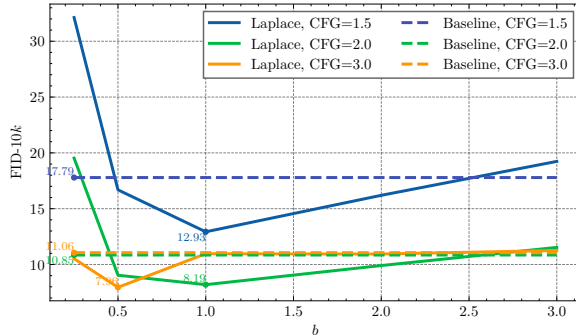
Laplace distribution, known for its simplicity and exponential decay from the center, is straightforward to implement. We leverage its symmetric nature and adjust the scale parameter to center the peak at the middle timestep. We conduct experiments with different Laplace distribution scales $b \in \{0.25, 0.5, 1.0, 2.0, 3.0\}$. The results are shown in Figure 3. The baseline with standard cosine schedule achieves FID score of 17.79 with CFG=1.5, 10.85 with CFG=2.0, and 11.06 with CFG=3.0 after 500K iterations. We can see that the model with Laplace distribution scale $b = 0.5$ achieves the best performance 7.96 with CFG=3.0, which is relatively **26.6%** better than the baseline.

Cauchy distribution is another heavy-tailed distribution that can be used for noise schedule design. The distribution is not symmetric when the location parameter is not 0. We conduct experiments with different Cauchy distribution parameters and the results are shown in Table 6. Cauchy(0, 0.5) means $\frac{1}{\pi} \frac{\gamma}{(\lambda-\mu)^2+\gamma^2}$ with $\mu = 0, \gamma = 0.5$. We can see that the model with $\mu = 0$ achieve better performance than the other two settings when fixing γ to 1. It means that the model with more probability mass around $\lambda = 0$ performs better than others biased to negative or positive directions.

Cosine Shifted (Hooeboom et al., 2023) is the shifted version of the standard cosine schedule. We evaluate the schedules with both positive and negative μ values to comprehensively assess its impact on model performance. Shifted with $\mu = 1$ achieves FID-10k score $\{19.34, 11.67, 11.13\}$ with CFG $\{1.5, 2.0, 3.0\}$. Results with shifted value $\mu = -1$ are $\{19.30, 11.48, 11.28\}$. Comparatively, both scenarios demonstrate inferior performance relative to the baseline cosine schedule ($\mu = 0$). Additionally, by examining the data presented in Table 6, we find concentrated on $\lambda = 0$ can best improve the results.

Noise Schedule	Cosine	Laplace
FID-10K	11.91	9.09 (-2.82)

Table 5: FID-10K results on ImageNet-512. All models are trained for 500K iterations.

Figure 3: FID-10K results on ImageNet-256 with location parameter μ fixed to 0 and different Laplace distribution scales b in $\{0.25, 0.5, 1.0, 2.0, 3.0\}$. Baseline denotes standard cosine schedule.

Cosine Scaled is also a modification of Cosine schedule. When $s = 1$, it becomes the standard Cosine version. $s > 1$ means sampling more heavily around $\lambda = 0$ while $s < 1$ means sampling more uniformly of all λ . We report related results in Table 7. Our experimental results reveal a clear trend: larger values of s ($s > 1$) consistently outperform the baseline, highlighting the benefits of focused sampling near $\lambda = 0$. However, it’s crucial to note that s should not be excessively large and must remain within a valid range to maintain stable training dynamics. For example, decreasing $1/s$ from 0.5 to 0.25 hurts the performance and cause the FID score to drop. Striking the right balance is key to optimizing performance. In our experiments, a model trained with $s = 2$ achieved a remarkable score of 8.04, representing a substantial **25.9%** improvement over the baseline.

The experiments with various noise schedules, including Laplace, Cauchy, Cosine Shifted, and Cosine Scaled, reveal a shared phenomenon: *models perform better when the noise distribution or schedule is concentrated around $\lambda = 0$* . For the Laplace distribution, a scale of $b = 0.5$ yielded the best performance, outperforming the baseline by 26.6%. In the case of the Cauchy distribution, models with a location parameter $\mu = 0$ performed better than those with μ values biased towards negative or positive directions. The Cosine Shifted schedule showed inferior performance when shifted away from $\mu = 0$, while the Cosine Scaled schedule demonstrated that larger values of s (sampling more heavily around $\lambda = 0$) consistently outperformed the baseline, with an optimal improvement of 25.9% at $s = 2$. This consistent trend suggests that focusing the noise distribution or schedule near $\lambda = 0$ is beneficial for model performance. While these different schedules take various mathematical forms, they all achieve similar optimal performance when given equivalent training budgets. The specific mathematical formulation is less crucial than the underlying design philosophy: increasing the sampling probability of intermediate noise levels. This principle provides a simple yet effective guideline for designing noise schedules.

$1/s$	1.3	1.1	0.5	0.25
CFG=1.5	39.74	22.60	12.74	15.83
CFG=2.0	23.38	12.98	8.04	8.64
CFG=3.0	13.94	11.16	11.02	8.26

Table 7: FID-10k results on ImageNet-256 with different scales of Cosine Scaled distribution.

4 RELATED WORK

Efficient Diffusion Training. The diffusion model uses a network with shared parameters to denoise different noise intensities. To improve training efficiency, P2 (Choi et al., 2022) and Min-SNR (Hang et al., 2023) propose different weighting schemes to prioritize important learning targets. On the architecture side, DiT (Peebles & Xie, 2023) introduces adaptive Layer Normalization with zero initialization, which was later extended to multi-modal scenarios in MM-DiT (Esser et al., 2024). In this work, we adopt the DiT architecture and focus on the importance sampling schedule.

Noise Schedule Design. The noise schedule design significantly impacts diffusion model training. While DDPM Ho et al. (2020) uses a linear schedule, Improved DDPM (Nichol & Dhariwal, 2021) proposes a cosine schedule to better approximate Gaussian noise at the highest noise level. Recent works Chen (2023); Hooeboom et al. (2023) suggest that the optimal noise schedule should be adapted according to image resolution.

A more detailed version of related works can be found in Appendix A.3.

5 CONCLUSION

In this paper, we present a novel method for enhancing the training of diffusion models by strategically redefining the noise schedule. Our theoretical analysis demonstrates that this approach is equivalent to performing importance sampling on the noise. Empirical results show that our proposed Laplace noise schedule, which focuses computational resources on mid-range noise levels, yields superior performance compared to adjusting loss weights under constrained computational budgets. This study not only contributes significantly to the development of efficient training techniques for diffusion models but also offers promising potential for future large-scale applications.

REFERENCES

- Yogesh Balaji, Seungjun Nah, Xun Huang, Arash Vahdat, Jiaming Song, Karsten Kreis, Miika Aittala, Timo Aila, Samuli Laine, Bryan Catanzaro, Tero Karras, and Ming-Yu Liu. ediff-i: Text-to-image diffusion models with ensemble of expert denoisers. *arXiv preprint arXiv:2211.01324*, 2022.
- Fan Bao, Shen Nie, Kaiwen Xue, Yue Cao, Chongxuan Li, Hang Su, and Jun Zhu. All are worth words: A vit backbone for diffusion models. *arXiv preprint arXiv:2209.12152*, 2022.
- Christopher M Bishop and Nasser M Nasrabadi. *Pattern recognition and machine learning*, volume 4. Springer, 2006.
- Tim Brooks, Bill Peebles, Connor Holmes, Will DePue, Yufei Guo, Li Jing, David Schnurr, Joe Taylor, Troy Luhman, Eric Luhman, Clarence Ng, Ricky Wang, and Aditya Ramesh. Video generation models as world simulators. 2024. URL <https://openai.com/research/video-generation-models-as-world-simulators>.
- Soravit Changpinyo, Piyush Sharma, Nan Ding, and Radu Soricut. Conceptual 12m: Pushing web-scale image-text pre-training to recognize long-tail visual concepts. In *Proceedings of the IEEE/CVF conference on computer vision and pattern recognition*, pp. 3558–3568, 2021.
- Ting Chen. On the importance of noise scheduling for diffusion models. *arXiv preprint arXiv:2301.10972*, 2023.
- Jooyoung Choi, Jungbeom Lee, Chaehun Shin, Sungwon Kim, Hyunwoo Kim, and Sungroh Yoon. Perception prioritized training of diffusion models. In *Proceedings of the IEEE/CVF Conference on Computer Vision and Pattern Recognition*, pp. 11472–11481, 2022.
- Katherine Crowson, Stefan Andreas Baumann, Alex Birch, Tanishq Mathew Abraham, Daniel Z Kaplan, and Enrico Shippole. Scalable high-resolution pixel-space image synthesis with hourglass diffusion transformers. In *Forty-first International Conference on Machine Learning*, 2024.
- Jia Deng, Wei Dong, Richard Socher, Li-Jia Li, Kai Li, and Li Fei-Fei. Imagenet: A large-scale hierarchical image database. In *2009 IEEE conference on computer vision and pattern recognition*, pp. 248–255. Ieee, 2009.
- Patrick Esser, Sumith Kulal, Andreas Blattmann, Rahim Entezari, Jonas Müller, Harry Saini, Yam Levi, Dominik Lorenz, Axel Sauer, Frederic Boesel, et al. Scaling rectified flow transformers for high-resolution image synthesis. *arXiv preprint arXiv:2403.03206*, 2024.
- Zhida Feng, Zhenyu Zhang, Xintong Yu, Yewei Fang, Lanxin Li, Xuyi Chen, Yuxiang Lu, Jiaxiang Liu, Weichong Yin, Shikun Feng, et al. Ernie-vilg 2.0: Improving text-to-image diffusion model with knowledge-enhanced mixture-of-denoising-experts. *arXiv preprint arXiv:2210.15257*, 2022.
- Shanghua Gao, Pan Zhou, Ming-Ming Cheng, and Shuicheng Yan. Masked diffusion transformer is a strong image synthesizer. In *Proceedings of the IEEE/CVF International Conference on Computer Vision*, pp. 23164–23173, 2023.
- Shuyang Gu, Dong Chen, Jianmin Bao, Fang Wen, Bo Zhang, Dongdong Chen, Lu Yuan, and Baining Guo. Vector quantized diffusion model for text-to-image synthesis. In *Proceedings of the IEEE/CVF conference on computer vision and pattern recognition*, pp. 10696–10706, 2022.
- Tiankai Hang, Shuyang Gu, Chen Li, Jianmin Bao, Dong Chen, Han Hu, Xin Geng, and Baining Guo. Efficient diffusion training via min-snr weighting strategy. In *Proceedings of the IEEE/CVF International Conference on Computer Vision (ICCV)*, pp. 7441–7451, October 2023.
- Jonathan Ho and Tim Salimans. Classifier-free diffusion guidance. In *NeurIPS 2021 Workshop on Deep Generative Models and Downstream Applications*, 2021.
- Jonathan Ho, Ajay Jain, and Pieter Abbeel. Denoising diffusion probabilistic models. *Advances in Neural Information Processing Systems*, 33:6840–6851, 2020.

- Jonathan Ho, Tim Salimans, Alexey A. Gritsenko, William Chan, Mohammad Norouzi, and David J. Fleet. Video diffusion models. In Alice H. Oh, Alekh Agarwal, Danielle Belgrave, and Kyunghyun Cho (eds.), *Advances in Neural Information Processing Systems*, 2022. URL https://openreview.net/forum?id=f3zNgKga_ep.
- Emiel Hoogeboom, Jonathan Heek, and Tim Salimans. simple diffusion: End-to-end diffusion for high resolution images. In *International Conference on Machine Learning*, pp. 13213–13232. PMLR, 2023.
- Tero Karras, Miika Aittala, Timo Aila, and Samuli Laine. Elucidating the design space of diffusion-based generative models. In Alice H. Oh, Alekh Agarwal, Danielle Belgrave, and Kyunghyun Cho (eds.), *Advances in Neural Information Processing Systems*, 2022. URL <https://openreview.net/forum?id=k7FuTOWMOc7>.
- Tero Karras, Miika Aittala, Jaakko Lehtinen, Janne Hellsten, Timo Aila, and Samuli Laine. Analyzing and improving the training dynamics of diffusion models. In *Proc. CVPR*, 2024.
- D. P. Kingma and J. Ba. Adam: A method for stochastic optimization. In *International Conference on Learning Representations*, 2014.
- Diederik Kingma, Tim Salimans, Ben Poole, and Jonathan Ho. Variational diffusion models. *Advances in neural information processing systems*, 34:21696–21707, 2021.
- Diederik P Kingma and Ruiqi Gao. Understanding diffusion objectives as the ELBO with simple data augmentation. In *Thirty-seventh Conference on Neural Information Processing Systems*, 2023. URL <https://openreview.net/forum?id=NnMEadcdyD>.
- Shanchuan Lin, Bingchen Liu, Jiashi Li, and Xiao Yang. Common diffusion noise schedules and sample steps are flawed. In *Proceedings of the IEEE/CVF winter conference on applications of computer vision*, pp. 5404–5411, 2024.
- Yaron Lipman, Ricky TQ Chen, Heli Ben-Hamu, Maximilian Nickel, and Matthew Le. Flow matching for generative modeling. In *The Eleventh International Conference on Learning Representations*, 2022.
- Xingchao Liu, Chengyue Gong, et al. Flow straight and fast: Learning to generate and transfer data with rectified flow. In *The Eleventh International Conference on Learning Representations*, 2022.
- Ziwei Liu, Ping Luo, Xiaogang Wang, and Xiaoou Tang. Deep learning face attributes in the wild. In *Proceedings of International Conference on Computer Vision (ICCV)*, December 2015.
- Alex Nichol, Heewoo Jun, Prafulla Dhariwal, Pamela Mishkin, and Mark Chen. Point-e: A system for generating 3d point clouds from complex prompts. *arXiv preprint arXiv:2212.08751*, 2022.
- Alexander Quinn Nichol and Prafulla Dhariwal. Improved denoising diffusion probabilistic models. In *International Conference on Machine Learning*, pp. 8162–8171. PMLR, 2021.
- William Peebles and Saining Xie. Scalable diffusion models with transformers. In *Proceedings of the IEEE/CVF International Conference on Computer Vision*, pp. 4195–4205, 2023.
- Adam Polyak, Amit Zohar, Andrew Brown, Andros Tjandra, Animesh Sinha, Ann Lee, Apoorv Vyas, Bowen Shi, Chih-Yao Ma, Ching-Yao Chuang, et al. Movie gen: A cast of media foundation models. *arXiv preprint arXiv:2410.13720*, 2024.
- Aditya Ramesh, Prafulla Dhariwal, Alex Nichol, Casey Chu, and Mark Chen. Hierarchical text-conditional image generation with clip latents. *arXiv preprint arXiv:2204.06125*, 2022.
- Robin Rombach, Andreas Blattmann, Dominik Lorenz, Patrick Esser, and Björn Ommer. High-resolution image synthesis with latent diffusion models. In *Proceedings of the IEEE/CVF Conference on Computer Vision and Pattern Recognition*, pp. 10684–10695, 2022.

- Chitwan Saharia, William Chan, Saurabh Saxena, Lala Li, Jay Whang, Emily Denton, Seyed Kamyar Seyed Ghasemipour, Raphael Gontijo-Lopes, Burcu Karagol Ayan, Tim Salimans, Jonathan Ho, David J. Fleet, and Mohammad Norouzi. Photorealistic text-to-image diffusion models with deep language understanding. In Alice H. Oh, Alekh Agarwal, Danielle Belgrave, and Kyunghyun Cho (eds.), *Advances in Neural Information Processing Systems*, 2022. URL <https://openreview.net/forum?id=08Yk-n5l2Al>.
- Tim Salimans and Jonathan Ho. Progressive distillation for fast sampling of diffusion models. In *International Conference on Learning Representations*, 2022. URL <https://openreview.net/forum?id=TIIdIXIpzhoI>.
- Uriel Singer, Adam Polyak, Thomas Hayes, Xi Yin, Jie An, Songyang Zhang, Qiyuan Hu, Harry Yang, Oron Ashual, Oran Gafni, Devi Parikh, Sonal Gupta, and Yaniv Taigman. Make-a-video: Text-to-video generation without text-video data. In *The Eleventh International Conference on Learning Representations*, 2023. URL <https://openreview.net/forum?id=nJfy1Dvgz1q>.
- Jiaming Song, Chenlin Meng, and Stefano Ermon. Denoising diffusion implicit models. In *International Conference on Learning Representations*, 2021.
- Zhicong Tang, Shuyang Gu, Chunyu Wang, Ting Zhang, Jianmin Bao, Dong Chen, and Baining Guo. Volumediffusion: Flexible text-to-3d generation with efficient volumetric encoder. *arXiv preprint arXiv:2312.11459*, 2023.
- Tengfei Wang, Bo Zhang, Ting Zhang, Shuyang Gu, Jianmin Bao, Tadas Baltrusaitis, Jingjing Shen, Dong Chen, Fang Wen, Qifeng Chen, et al. Rodin: A generative model for sculpting 3d digital avatars using diffusion. *arXiv preprint arXiv:2212.06135*, 2022.
- S. Yang, J. Sohl-Dickstein, D. P. Kingma, A. Kumar, S. Ermon, and B. Poole. Score-based generative modeling through stochastic differential equations. In *International Conference on Learning Representations*, 2021.
- Xuanlei Zhao, Zhongkai Zhao, Ziming Liu, Haotian Zhou, Qianli Ma, and Yang You. Opendit: An easy, fast and memory-efficient system for dit training and inference. <https://github.com/NUS-HPC-AI-Lab/OpenDiT>, 2024.

A APPENDIX

A.1 DETAILED IMPLEMENTATION FOR NOISE SCHEDULE

We provide a simple PyTorch implementation for the Laplace noise schedule and its application in training. This example can be adapted to other noise schedules, such as the Cauchy distribution, by replacing the `laplace_noise_schedule` function. The model accepts noisy samples \mathbf{x}_t , timestep t , and an optional condition tensor \mathbf{c} as inputs. This implementation supports prediction of $\{\mathbf{x}_0, \mathbf{v}, \epsilon\}$.

```

1 import torch
2
3
4 def laplace_noise_schedule(mu=0.0, b=0.5):
5     # refer to Table 1
6     lmb = lambda t: mu - b * torch.sign(0.5 - t) * \
7         torch.log(1 - 2 * torch.abs(0.5 - t))
8     snr_func = lambda t: torch.exp(lmb(t))
9     alpha_func = lambda t: torch.sqrt(snr_func(t) / (1 + snr_func(t)))
10    sigma_func = lambda t: torch.sqrt(1 / (1 + snr_func(t)))
11
12    return alpha_func, sigma_func
13
14
15 def training_losses(model, x, timestep, condition, noise=None,
16                    predict_target="v", mu=0.0, b=0.5):
17
18     if noise is None:
19         noise = torch.randn_like(x)
20
21     alpha_func, sigma_func = laplace_noise_schedule(mu, b)
22     alphas = alpha_func(timestep)
23     sigmas = sigma_func(timestep)
24
25     # add noise to sample
26     x_t = alphas.view(-1, 1, 1, 1) * x + sigmas.view(-1, 1, 1, 1) * noise
27     # velocity
28     v_t = alphas.view(-1, 1, 1, 1) * noise - sigmas.view(-1, 1, 1, 1) * x
29
30     model_output = model(x_t, timestep, condition)
31     if predict_target == "v":
32         loss = (v_t - model_output) ** 2
33     elif predict_target == "x0":
34         loss = (x - model_output) ** 2
35     else: # predict_target == "noise":
36         loss = (noise - model_output) ** 2
37
38     return loss.mean()

```

A.2 DETAILS FOR PROPOSED LAPLACE AND CAUCHY DESIGN

For a Laplace distribution with location parameter μ and scale parameter b , the probability density function (PDF) is given by:

$$p(\lambda) = \frac{1}{2b} \exp\left(-\frac{|\lambda - \mu|}{b}\right) \quad (7)$$

The cumulative distribution function (CDF) can be derived as follows:

$$\begin{aligned}
1 - t &= \int_{-\infty}^{\lambda} p(x) dx \\
&= \int_{-\infty}^{\lambda} \frac{1}{2b} \exp\left(-\frac{|x - \mu|}{b}\right) dx \\
&= \frac{1}{2} \left(1 + \operatorname{sgn}(\lambda - \mu) \left(1 - \exp\left(-\frac{|\lambda - \mu|}{b}\right)\right)\right)
\end{aligned}$$

To obtain λ as a function of t , we solve the inverse function:

$$\lambda = \mu - b \operatorname{sgn}(0.5 - t) \ln(1 - 2|t - 0.5|)$$

For a Cauchy distribution with location parameter μ and scale parameter γ , the PDF is given by:

$$f(\lambda; \mu, \gamma) = \frac{1}{\pi\gamma} \left[1 + \left(\frac{\lambda - \mu}{\gamma}\right)^2\right]^{-1} \quad (8)$$

The corresponding CDF is:

$$F(\lambda; \mu, \gamma) = \frac{1}{2} + \frac{1}{\pi} \arctan\left(\frac{\lambda - \mu}{\gamma}\right) \quad (9)$$

To derive $\lambda(t)$, we proceed as follows:

$$1 - t = F(\lambda; \mu, \gamma) \quad (10)$$

$$1 - t = \frac{1}{2} + \frac{1}{\pi} \arctan\left(\frac{\lambda - \mu}{\gamma}\right) \quad (11)$$

$$t = \frac{1}{2} - \frac{1}{\pi} \arctan\left(\frac{\lambda - \mu}{\gamma}\right) \quad (12)$$

Solving for λ , we obtain:

$$\lambda(t) = \mu + \gamma \tan\left(\frac{\pi}{2}(1 - 2t)\right) \quad (13)$$

A.3 DETAILED VERSION OF RELATED WORKS

Efficient Diffusion Training. Generally speaking, the diffusion model uses a network with shared parameters to denoise different noise intensities. However, the different noise levels may introduce conflicts during training, which makes the convergence slow. P2 (Choi et al., 2022) improves image generation performance by prioritizing the learning of perceptually rich visual concepts during training through a redesigned weighting scheme. Min-SNR (Hang et al., 2023) seeks the Pareto optimal direction for different tasks, achieves better convergence on different predicting targets. HDiT (Crowson et al., 2024) propose a soft version of Min-SNR to further improve the efficiency on high resolution image synthesis. Stable Diffusion 3 (Esser et al., 2024) puts more sampling weight on the middle timesteps by multiplying the distribution of logit normal distribution.

On the other hand, architecture modification is also explored to improve diffusion training. DiT (Peebles & Xie, 2023) proposes adaptive Layer Normalization with zero initialization to improve the training of Transformer architectures. Building upon this design, MM-DiT (Esser et al., 2024) extends the approach to a multi-modal framework (text to image) by incorporating separate sets of weights for each modality. HDiT (Crowson et al., 2024) uses a hierarchical transformer structure for efficient, linear-scaling, high-resolution image generation. A more robust ADM UNet

with better training dynamics is proposed in EDM2 (Karras et al., 2024) by preserving activation, weight, and update magnitudes. In this work, we directly adopt the design from DiT (Peebles & Xie, 2023) and focus on investigating the importance sampling schedule in diffusion models.

Noise Schedule Design for Diffusion Models. The design of the noise schedule plays a critical role in training diffusion models. In DDPM, Ho et al. (2020) propose linear schedule for the noise level, which was later adopted by Stable Diffusion (Rombach et al., 2022) version 1.5 and 2.0. However, the linear noise schedule introduces signal leakage at the highest noise step (Lin et al., 2024; Tang et al., 2023), hindering performance when sampling starts from a Gaussian distribution. Improved DDPM (Nichol & Dhariwal, 2021) introduces a cosine schedule aimed at bringing the sample with the highest noise level closer to pure Gaussian noise. EDM (Karras et al., 2022) proposes a new continuous framework and make the logarithm of noise intensity sampled from a Gaussian distribution. Flow matching with optimal transport (Lipman et al., 2022; Liu et al., 2022) linearly interpolates the noise and data point as the input of flow-based models. Chen (2023) underscored the need for adapting the noise schedule according to the image resolution. Hoogeboom et al. (2023) found that cosine schedule exhibits superior performance for images of 32×32 and 64×64 resolutions and propose to shift the cosine schedule to train on images with higher resolutions.

A.4 COMBINATION BETWEEN NOISE SCHEDULE AND TIMESTEP IMPORTANCE SAMPLING

We observe that incorporating importance sampling of timesteps into the cosine schedule bears similarities to the Laplace schedule. Typically, the distribution of timestep t is uniform $\mathcal{U}[0, 1]$. To increase the sampling frequency of middle-level timesteps, we propose modifying the sampling distribution to a simple polynomial function:

$$p(t') = \begin{cases} C \cdot t'^n, & t' < \frac{1}{2} \\ C \cdot (1 - t')^n, & t' \geq \frac{1}{2}, \end{cases} \quad (14)$$

where $C = (n + 1)2^n$ is the normalization factor ensuring that the cumulative distribution function (CDF) equals 1 at $t = 1$.

To sample from this distribution, we first sample t uniformly from $(0, 1)$ and then map it using the following function:

$$t' = \begin{cases} \left(\frac{1}{2}\right)^{\frac{n}{n+1}} t^{\frac{1}{n+1}}, & t < \frac{1}{2} \\ 1 - \left(\frac{1}{2}\right)^{\frac{n}{n+1}} (1 - t)^{\frac{1}{n+1}}, & t \geq \frac{1}{2}, \end{cases} \quad (15)$$

We incorporate the polynomial sampling of t into the cosine schedule $\lambda = -2 \log \tan \frac{\pi t}{2}$, whose inverse function is $t = \frac{2}{\pi} \arctan \exp\left(-\frac{\lambda}{2}\right)$. Let us first consider the situation where $t < \frac{1}{2}$:

$$\left(\frac{1}{2}\right)^{\frac{n}{n+1}} t^{\frac{1}{n+1}} = \frac{2}{\pi} \arctan \exp\left(-\frac{\lambda}{2}\right) \quad (16)$$

$$t = 2^n \left(\frac{2}{\pi} \arctan \exp\left(-\frac{\lambda}{2}\right)\right)^{n+1} \quad (17)$$

We then derive the expression with respect to $d\lambda$:

$$\frac{dt}{d\lambda} = 2^n \left(\frac{2}{\pi}\right)^{n+1} (n + 1) \left(\arctan \exp\left(-\frac{\lambda}{2}\right)\right)^n \frac{1}{1 + \exp(-\lambda)} \frac{1}{-2} \exp(-\lambda/2) \quad (18)$$

$$p(\lambda) = (n + 1) \frac{4^n}{\pi^{(n+1)}} \arctan^n \exp\left(-\frac{\lambda}{2}\right) \frac{\exp(-\frac{1}{2}\lambda)}{1 + \exp(-\lambda)} \quad (19)$$

$$(20)$$

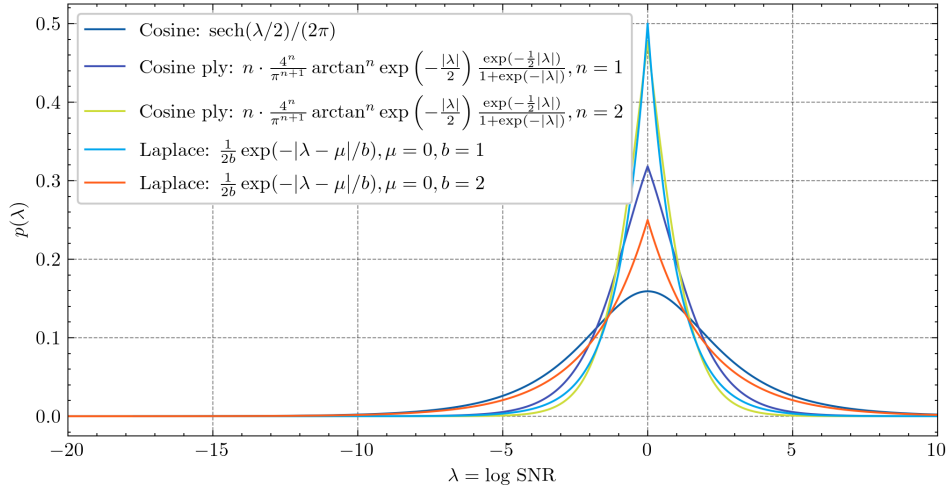


Figure 4: Visualization of $p(\lambda)$ for Laplace schedule and cosine schedule with polynomial timestep sampling.

Considering symmetry, we obtain the final distribution with respect to λ as follows:

$$p(\lambda) = (n+1) \frac{4^n}{\pi^{n+1}} \arctan^n \exp\left(-\frac{|\lambda|}{2}\right) \frac{\exp(-\frac{1}{2}|\lambda|)}{1 + \exp(-|\lambda|)} \quad (21)$$

We visualize the schedule discussed above and compare it with Laplace schedule in Figure 4. We can see that $b = 1$ for Laplace and $n = 2$ for cosine-ply matches well. We also conduct experiments on such schedule and present results in Table 8. They perform similar and both better than the standard cosine schedule.

We visualize the schedules discussed above and compare them with the Laplace schedule in Figure 4. The results demonstrate that Laplace with $b = 1$ and cosine-ply with $n = 2$ exhibit a close correspondence. To evaluate the performance of these schedules, we conducted experiments and present the results in Table 8. Both the Laplace and cosine-ply schedules show similar performance, and both outperform the standard cosine schedule.

Iterations	100,000	200,000	300,000	400,000	500,000
Cosine-ply ($n = 2$)	28.65	13.77	10.06	8.69	7.98
Laplace ($b = 1$)	28.89	13.90	10.17	8.85	8.19

Table 8: Performance comparison of cosine-ply ($n = 2$) and Laplace ($\mu = 1$) schedules over different iteration counts

A.5 FLOW MATCHING WITH LOGIT-NORMAL SAMPLING

In Stable Diffusion 3 (Esser et al., 2024) and Movie Gen (Polyak et al., 2024), logit-normal sampling is applied to improve the training efficiency of flow models. To better understand this approach, we present a detailed derivation from the logit-normal distribution to the probability density function of $\log\text{SNR } \lambda$.

Let the Logit transformation $X = \text{logit}(t)$ of random variable t follow a normal distribution:

$$X \sim \mathcal{N}(\mu, \sigma^2) \quad (22)$$

Then, the probability density function of t is:

$$p(t; \mu, \sigma) = \frac{1}{\sigma \cdot t \cdot (1-t) \cdot \sqrt{2\pi}} \exp\left(-\frac{(\text{logit}(t) - \mu)^2}{2\sigma^2}\right), \quad t \in (0, 1) \quad (23)$$

where $\text{logit}(t) = \log\left(\frac{t}{1-t}\right)$, and μ and σ are constants.

Consider the variable transformation:

$$\lambda = 2 \log\left(\frac{1-t}{t}\right) \quad (24)$$

Our goal is to find the probability density function $p(\lambda)$ of random variable λ .

First, we solve for t in terms of λ :

$$\begin{aligned} \frac{\lambda}{2} &= \log\left(\frac{1-t}{t}\right) \\ e^{\frac{\lambda}{2}} &= \frac{1-t}{t} \\ 1-t &= te^{\frac{\lambda}{2}} \\ 1 &= t\left(1+e^{\frac{\lambda}{2}}\right) \\ t(\lambda) &= \frac{1}{1+e^{\frac{\lambda}{2}}} \end{aligned}$$

Next, we calculate the Jacobian determinant $\left|\frac{dt}{d\lambda}\right|$:

$$\begin{aligned} t(\lambda) &= \frac{1}{1+e^{\frac{\lambda}{2}}} \\ \frac{dt}{d\lambda} &= -\frac{e^{\frac{\lambda}{2}} \cdot \frac{1}{2}}{(1+e^{\frac{\lambda}{2}})^2} \\ \left|\frac{dt}{d\lambda}\right| &= \frac{e^{\frac{\lambda}{2}}}{2(1+e^{\frac{\lambda}{2}})^2} \end{aligned}$$

Using the variable transformation formula:

$$p(\lambda) = p(t(\lambda); \mu, \sigma) \cdot \left|\frac{dt}{d\lambda}\right| \quad (25)$$

We calculate $p(t(\lambda); \mu, \sigma)$:

$$\begin{aligned} \text{logit}(t(\lambda)) &= \log\left(\frac{t(\lambda)}{1-t(\lambda)}\right) = \log\left(\frac{\frac{1}{1+e^{\frac{\lambda}{2}}}}{\frac{e^{\frac{\lambda}{2}}}{1+e^{\frac{\lambda}{2}}}}\right) = -\frac{\lambda}{2} \\ p(t(\lambda); \mu, \sigma) &= \frac{(1+e^{\frac{\lambda}{2}})^2}{\sigma e^{\frac{\lambda}{2}} \sqrt{2\pi}} \exp\left(-\frac{(\mu + \frac{\lambda}{2})^2}{2\sigma^2}\right) \end{aligned}$$

Multiplying by the Jacobian determinant:

$$\begin{aligned} p(\lambda) &= \frac{(1+e^{\frac{\lambda}{2}})^2}{\sigma e^{\frac{\lambda}{2}} \sqrt{2\pi}} \exp\left(-\frac{(\mu + \frac{\lambda}{2})^2}{2\sigma^2}\right) \cdot \frac{e^{\frac{\lambda}{2}}}{2(1+e^{\frac{\lambda}{2}})^2} \\ &= \frac{1}{2\sigma\sqrt{2\pi}} \exp\left(-\frac{(\lambda + 2\mu)^2}{8\sigma^2}\right) \end{aligned}$$

Therefore, the probability density function of λ is:

$$p(\lambda) = \frac{1}{2\sigma\sqrt{2\pi}} \exp\left(-\frac{(\lambda + 2\mu)^2}{8\sigma^2}\right), \quad \lambda \in (-\infty, +\infty) \quad (26)$$

This shows that λ follows a normal distribution with mean -2μ and variance $4\sigma^2$:

$$\lambda \sim \mathcal{N}(-2\mu, 4\sigma^2) \tag{27}$$

The mean and variance are:

$$\begin{aligned} \mathbb{E}[\lambda] &= -2\mu \\ \text{Var}(\lambda) &= 4\sigma^2 \end{aligned}$$

To verify normalization, we integrate $p(\lambda)$ over its domain:

$$\begin{aligned} \int_{-\infty}^{+\infty} p(\lambda) d\lambda &= \int_{-\infty}^{+\infty} \frac{1}{2\sigma\sqrt{2\pi}} \exp\left(-\frac{(\lambda + 2\mu)^2}{8\sigma^2}\right) d\lambda \\ \text{Let } z &= \frac{\lambda + 2\mu}{2\sqrt{2}\sigma} \Rightarrow d\lambda = 2\sqrt{2}\sigma dz \\ &= \frac{2\sqrt{2}\sigma}{2\sigma\sqrt{2\pi}} \int_{-\infty}^{+\infty} e^{-z^2} dz \\ &= \frac{1}{\sqrt{\pi}} \cdot \sqrt{\pi} = 1 \end{aligned}$$

Thus, $p(\lambda)$ satisfies the normalization condition for probability density functions.

We compare the standard cosine schedule (Nichol & Dhariwal, 2021), Flow Matching (Liu et al., 2022; Lipman et al., 2022), and Flow Matching with Logit-normal sampling (Esser et al., 2024; Polyak et al., 2024). The probability density functions of these schedules are visualized in Figure 5. Our analysis reveals that Flow Matching with Logit-normal sampling concentrates more probability mass around $\lambda = 0$ compared to both the standard Cosine and Flow Matching schedules, resulting in improved training efficiency (Esser et al., 2024; Polyak et al., 2024).

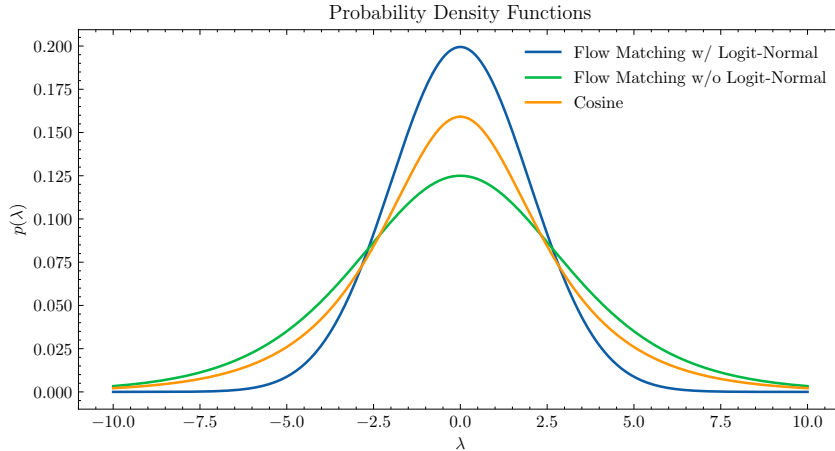


Figure 5: Comparison of probability density functions for different flow matching approaches. The plot shows three distributions: Flow Matching with Logit-Normal sampling (blue), Flow Matching without Logit-Normal sampling (green), and the Cosine schedule (orange).

A.6 IMPORTANCE OF TIME INTERVALS

To investigate the significance of training intervals, we conducted controlled experiments using a simplified setup. We divided the time range $(0, 1)$ into four equal segments: $\text{bin}_i = (\frac{i}{4}, \frac{i+1}{4})$, $i = 0, 1, 2, 3$. We first trained a base model M over the complete range $(0, 1)$ for 1M iterations, then fine-tuned it separately on each bin for 140k iterations to obtain four specialized checkpoints \mathbf{m}_i , $i = 0, 1, 2, 3$.

For evaluation, we designed experiments using both the base model M and fine-tuned checkpoints m_i . To assess the importance of each temporal segment, we selectively employed the corresponding fine-tuned checkpoint during its specific interval while maintaining the base model for remaining intervals. For example, when evaluating bin_0 , we used m_0 within its designated interval and M elsewhere.

The FID results across these four experimental configurations are presented in Figure 6. Our analysis reveals that optimizing intermediate timesteps (bin_1 and bin_2) yields superior performance, suggesting the critical importance of these temporal regions in the diffusion process.

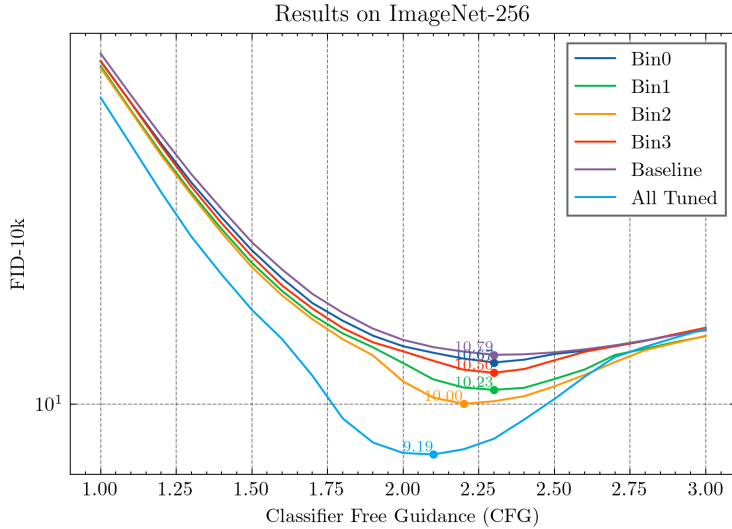


Figure 6: Comparative analysis of interval-specific fine-tuning effects. When sampling within interval $(\frac{1}{4}, \frac{2}{4})$, “Bin1” indicates the use of fine-tuned weights m_1 , while M is used for other intervals. “Baseline” represents the use of base model M throughout all intervals, and “All Tuned” denotes the application of interval-specific fine-tuned models within their respective ranges.

A.7 IMPORTANCE SAMPLING AS LOSS WEIGHT

We investigate the comparative effectiveness of our approach when applied as a noise schedule versus a loss weighting mechanism. We adopt Equation 21 as our primary noise schedule due to its foundation in the cosine schedule and demonstrated superior FID performance. To evaluate its versatility, we reformulate the importance sampling as a loss weighting strategy and compare it against established weighting schemes, including Min-SNR and Soft-Min-SNR.

	Cosine	Cosine-Ply ($n=2$)	Min-SNR	Soft-Min-SNR	Cosine-Ply as weight
FID-10K	10.85	7.98	9.70	9.07	8.88

Table 9: Quantitative comparison of different noise scheduling strategies and loss weighting schemes. Lower FID scores indicate better performance.

Figure 7 illustrates the loss weight derived from Cosine-Ply ($n=2$) schedule alongside Min-SNR and Soft-Min-SNR. We can observe that under the setting of predict target as v , Min-SNR and Soft-Min-SNR can be seemed as putting more weight on intermediate levels, aligning with our earlier findings on the importance of middle-level noise densities.

A.8 ADDITIONAL EXPERIMENTS ON OTHER DATASETS

ImageNet, comprising over one million natural images, has been widely adopted as a benchmark dataset for validating improvements in diffusion models (Peebles & Xie, 2023; Karras et al., 2024).

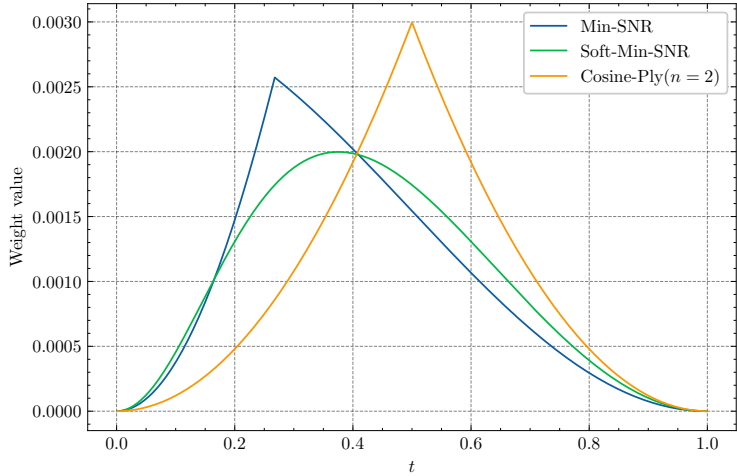


Figure 7: Visualization of different loss weight schemes.

In addition to ImageNet, we evaluate our approach on the CelebA (Liu et al., 2015) dataset (64×64 resolution in pixel space), which consists of face images. We employ a DiT architecture (12 layers, embedding dimension of 512, 8 attention heads, and patch size of 4) using different noise schedules. This is an unconditional generation setting within a single domain. We present FID results as follows:

FID ↓	100k	150k
cosine	10.0696	7.93795
Laplace (ours)	7.93795	6.58359

Table 10: FID scores on CelebA dataset at different training iterations

We also follow Stable Diffusion 3 (Esser et al., 2024), train on a more complicated dataset CC12M (Changpinyo et al., 2021) dataset (over 12M image-text pairs) and report the FID results here. We download the dataset using `webdataset`. We train a DiT-base model using CLIP as text conditioner. The images are cropped and resized to 256×256 resolution, compressed to $32 \times 32 \times 4$ latents and trained for 200k iterations at batch size 256.

FID ↓	200k
cosine	58.3619
Laplace (ours)	54.3492 (-4.0127)

Table 11: FID scores on CC12M dataset at 200k iterations

Our method demonstrated strong generalization capabilities across both unconditional image generation using the CelebA dataset and text-to-image generation using the CC12M dataset.

A.9 ADDITIONAL VISUAL RESULTS

We present additional visual results in Figure 8 to demonstrate the differences in generation quality between models trained with Cosine and our proposed Laplace schedule. Each case presents two rows of outputs, where the upper row shows results from the cosine schedule and the lower row displays results from our Laplace schedule. Each row contains five images corresponding to models trained for 100k, 200k, 300k, 400k, and 500k iterations, illustrating the progression of generation quality across different training stages. For each case, the initial noise inputs are identical. As shown in the results, our method achieves faster convergence in both basic object formation (at

100k iterations) and fine detail refinement, demonstrating superior learning efficiency throughout the training process.

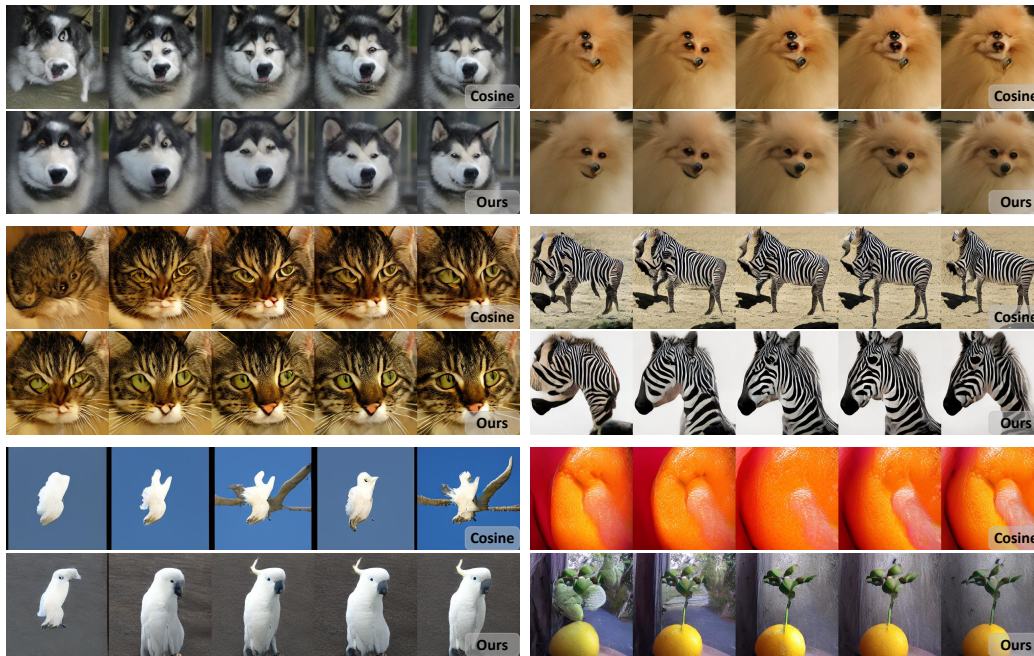


Figure 8: Visual comparison of results generated by model trained by cosine schedule and our proposed Laplace. For each case, the above row is generated by cosine schedule, the below is generated by Laplace. The 5 images from left to right represents the results generated by the model trained for 100k, 200k, 300k, 400k, and 500k iterations.